


# Influence of pore morphology on the diffusion of water in triblock copolymer membranes

Cite as: J. Chem. Phys. **152**, 014904 (2020); <https://doi.org/10.1063/1.5128119>

Submitted: 17 September 2019 . Accepted: 11 December 2019 . Published Online: 07 January 2020

Dipak Aryal,  Michael P. Howard,  Rituparna Samanta, Segolene Antoine,  Rachel Segalman,  Thomas M. Truskett, and  Venkat Ganesan



View Online



Export Citation



CrossMark

## ARTICLES YOU MAY BE INTERESTED IN

[Impact of cross-linking of polymers on transport of salt and water in polyelectrolyte membranes: A mesoscopic simulation study](#)

The Journal of Chemical Physics **149**, 224902 (2018); <https://doi.org/10.1063/1.5057708>

[Inverse methods for design of soft materials](#)

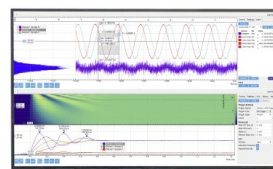
The Journal of Chemical Physics **152**, 140902 (2020); <https://doi.org/10.1063/1.5145177>

[Structure and phase behavior of polymer-linked colloidal gels](#)

The Journal of Chemical Physics **151**, 124901 (2019); <https://doi.org/10.1063/1.5119359>

Challenge us.

What are your needs for  
periodic signal detection?



Zurich  
Instruments

# Influence of pore morphology on the diffusion of water in triblock copolymer membranes

Cite as: J. Chem. Phys. 152, 014904 (2020); doi: 10.1063/1.5128119

Submitted: 17 September 2019 • Accepted: 11 December 2019 •

Published Online: 7 January 2020



View Online



Export Citation



CrossMark

Dipak Aryal,<sup>1</sup> Michael P. Howard,<sup>1</sup>  Rituparna Samanta,<sup>1</sup>  Segolene Antoine,<sup>2</sup> Rachel Segalman,<sup>2</sup>   
Thomas M. Truskett,<sup>1</sup>  and Venkat Ganesan<sup>1,a)</sup> 

## AFFILIATIONS

<sup>1</sup>Department of Chemical Engineering, University of Texas at Austin, Austin, Texas 78712, USA

<sup>2</sup>Department of Chemical Engineering, University of California, Santa Barbara, California 93106, USA

<sup>a)</sup> Author to whom correspondence should be addressed: [venkat@che.utexas.edu](mailto:venkat@che.utexas.edu)

## ABSTRACT

Understanding the transport properties of water in self-assembled block copolymer morphologies is important for furthering the use of such materials as water-purifying membranes. In this study, we used coarse-grained dissipative particle dynamics simulations to clarify the influence of pore morphology on the self-diffusion of water in linear-triblock-copolymer membranes. We considered representative lamellar, cylindrical, and gyroid morphologies and present results for both the global and local diffusivities of water in the pores. Our results suggest that the diffusivity of water in the confined, polymer-coated pores differs from that in the unconfined bulk. Explicitly, in confinement, the mobility of water is reduced by the hydrodynamic friction arising from the hydrophilic blocks coating the pore walls. We demonstrate that in lamella and cylindrical morphologies, the latter effects can be rendered as a universal function of the pore size relative to the brush height of the hydrophilic blocks.

Published under license by AIP Publishing. <https://doi.org/10.1063/1.5128119>

## I. INTRODUCTION

Morphologies with continuous nanoporous pathways percolated in one or more dimensions are important for technologies such as water purification membranes and fuel cells. In this context, particular interest has arisen in block copolymers (BCPs) because they self-assemble into rich nanostructured morphologies, such as lamellae, cylinders, and gyroids, with nanometer-sized domains.<sup>1,2</sup> In such applications as desalination and reverse osmosis, the dynamics and structure of water and other permeants in the polymer membranes are expected to be perturbed by the morphology, pore size, surface chemistry, and the interaction with the blocks that have preferable water selectivity. An understanding of the transport properties of water with regard to these features is crucial to enable the design and optimization of such membranes.

Relatively few studies<sup>3–5</sup> have investigated the influence of morphology on the transport of small molecules and solvent in the block copolymer. Winey and co-workers examined the morphology and properties of a series of pentablock copolymer membranes and demonstrated an impact of the morphology on water sorption of

the membrane.<sup>6,7</sup> More recently, Oparaji *et al.*<sup>5</sup> quantified the effect of morphology on crystallization, water sorption, and transport in poly(styrene-*b*-ethylene oxide) block copolymers. Interestingly, they found that at the same thermodynamic activity of water, the water diffusivity in cylindrical morphologies was approximately half of that of the lamellar phases.

There are even fewer theoretical or computer simulation studies of solvent transport in *periodic*, self-assembled block copolymer membranes. Much of the work has been inspired by lithium ion battery applications<sup>8–10</sup> and has focused on ion transport in dry polymer electrolytes. For instance, Sethuraman *et al.*<sup>11,12</sup> compared ion transport mechanisms in the lamellar phase of the salt-doped poly(styrene-*b*-ethylene oxide) block copolymer to those in the corresponding homopolymers and demonstrated the importance of interfacial segmental dynamics and ion partitioning in the former. Recently, Shen *et al.*<sup>13</sup> used a random walk model to probe diffusion of a tracer in lamellar, cylindrical, and gyroid nanostructures of block copolymers. They (and others) have shown that the diffusion of ions is influenced mainly by the tortuosity of the morphologies.<sup>14,15</sup>

While the above-discussed computational studies have shed light on some of the factors that influence ion transport in dry block copolymers, it is not straightforward to translate such understanding to solvated membranes. Indeed, since ion transport in dry block copolymers occurs through a polymer-segment-mediated hopping process, the resulting ion mobilities are influenced by the impact of polymer morphology on local polymer segmental dynamics.<sup>12</sup> In contrast, the solvent dynamics are expected to involve (in addition to the polymer dynamics) a strong role for interactions with the hydrophilic polymer domains exposed to the solvent. To our knowledge, there has been no prior study that has computationally investigated the influence of morphology on the structural and dynamical properties of water in confined geometries such as lamellae, cylinders, and gyroids that arise from the self-assembly of block copolymers.

The motivation for our present study draws from recent experimental efforts in our groups that aim to utilize the self-assembly of block copolymers to create functionalized nanoporous materials for water purification. Specifically, our framework, as shown in Fig. 1, envisions the use of self-assembled morphologies of poly(styrene-*b*-ethylene oxide-*b*-lactide) (PS-PEO-PLA) linear triblock copolymers, in which the PLA block is etched out<sup>16,17</sup> to create nanoporous membranes and facilitate transport of water. Such experimental pursuits have raised the following questions: (a) Do the dynamical properties of water exhibit a dependence on the morphology of the nanoporous membrane? (b) How does confinement influence the local and global transport properties of the solvent molecules? (c) How are the structural and dynamical characteristics of water influenced by the chain length of PEO blocks in the pore?

To address the above questions, we used computer simulations to investigate the role of the nanopore morphology and the influence of the PEO blocks that coat their walls on the transport properties of water. We adopted a coarse-grained model for the PS-PEO-PLA triblock copolymers [Fig. 1(a)] based on the dissipative particle dynamics (DPD)<sup>18–21</sup> method, which has proven to be an efficient tool for studying the structural and dynamical properties of polymer solutions and melts at long time and length scales.<sup>22</sup> We mimicked the experimental strategy with the simulations to create

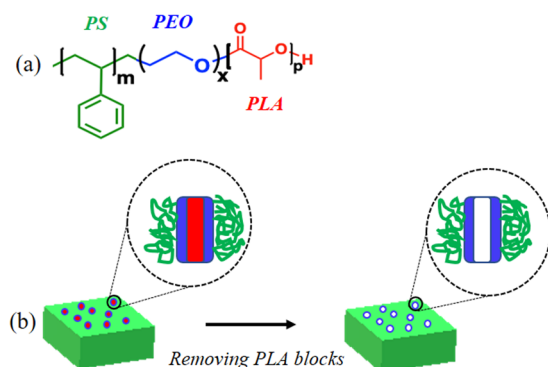


**FIG. 1.** (a) Chemical structure of poly(styrene)-*b*-ethylene oxide-*b*-lactide triblock copolymer. (b) The schematic framework for the process of creating a pore in the membranes of triblock copolymers. Representative color: green for the PS block, blue for the PEO block, and red for the PLA block.

unit cells of nanoporous lamellar, cylindrical, and gyroid morphologies. Such pores were then filled with water to probe their transport properties.

The rest of the article is organized as follows. Details of the simulation methodology and characterization methods are given in Sec. II. Results and discussion are presented in Sec. III. We provide evidence for the influence of the morphology and the water selective block on the transport of water. We rationalize the latter results by discussing phenomena that arise in the context of solvent dynamics near polymer brushes. We conclude with a summary of our findings in Sec. IV.

## II. MODEL AND METHODOLOGY

### A. DPD simulations

All the reported simulations were carried out for a constant number of total particles, fixed volume, and temperature using the LAMMPS package.<sup>23</sup> To model the self-assembled morphologies arising in the triblock copolymer, we employed a coarse-grained DPD framework, proposed by Hoogerbrugge and Koelman<sup>24</sup> and outlined by Groot and Warren,<sup>18</sup> to study the self-assembled phases of copolymers.<sup>19,26,27</sup> All particles interact via three pairwise forces: a soft repulsive force, a velocity dependent drag force, and a random force. The soft repulsive force was computed from the potential<sup>18</sup>

$$U(r) = \begin{cases} \frac{a_{ij}(r-r_c)^2}{2r_c}, & r \leq r_c, \\ 0, & r > r_c, \end{cases} \quad (1)$$

where  $r$  is the distance between particles  $i$  and  $j$ ,  $r_c$  is the pairwise truncation distance for the interaction, and  $a_{ij}$  is the DPD interaction parameter. Following standard approaches to DPD simulations<sup>18,19,27</sup> with the reduced particle-number density of  $\rho r_c^3 = 3$ , the repulsive parameters between different beads  $a_{ij}$  are related to the Flory-Huggins parameter ( $\chi_{ij}$ ) as

$$a_{ij} \approx a_{ii} + 3.27\chi_{ij}. \quad (2)$$

The  $\chi_{ij}$  parameters were adopted from experimental studies (see Table S1).<sup>28,29</sup> Following an approach similar to that proposed in Ref. 30, we adopted a coarse-graining framework in which one bead represented four water molecules ( $N_m = 4$ ), giving a bead volume comparable to the size of a monomer in our block copolymers. We set the same-type repulsion parameters  $a_{ii}$  to  $106.1 k_B T / r_c$  in order to match the compressibility of the DPD fluid to that of water.<sup>30</sup> A full table of repulsion parameters between same or different beads is presented in the [supplementary material](#). The drag and friction forces satisfied the fluctuation-dissipation theorem for a friction factor  $\gamma = 4.5 m \tau^{-1}$  to maintain constant temperature at  $T$ , with the time unit  $\tau = r_c \sqrt{m / k_B T}$  and  $m$  being the mass of a bead.<sup>18,19</sup>

### B. Methods for modeling polymers, creating pores, and adding water particles

The schematic structures of the PS-PEO-PLA linear triblock copolymers and the coarse-grained representations adopted in our

study are depicted in Fig. 1(a). Specifically, we divided the chemical units of the polymer into three types of DPD beads, corresponding to the styrene, ethylene oxide, and lactic acid units. The mass of each bead was taken as a unit mass, and the beads in the chains were connected by harmonic bonds with spring constant  $K = 50 k_B T / r_c^2$  and equilibrium distance  $r_o = 0.85 r_c$ . Based on guidance from theoretical predictions<sup>31</sup> and the DPD framework<sup>26</sup> for the morphologies of triblock copolymers, we considered the block lengths of each block with the following compositions: (i) lamellae ( $f_{PS} = 0.4$ ,  $f_{PEO} = 0.28$ , and  $f_{PLA} = 0.32$ ); (ii) cylinder ( $f_{PS} = 0.70$ ,  $f_{PEO} = 0.04$ , and  $f_{PLA} = 0.26$ ); (iii) gyroid ( $f_{PS} = 0.65$ ,  $f_{PEO} = 0.04$ , and  $f_{PLA} = 0.31$ ). We simulated 1000 polymer chains each with 100 beads in the systems in a cubic simulation cell with an edge length of  $\sim 32.2 r_c$ . Periodic boundary conditions were applied in all directions.

Before adding water particles into the system, the lamellae, cylinder, and gyroid morphologies were obtained by simulating the corresponding systems from random initial conditions. In correspondence with the experimental strategy,<sup>16,17</sup> after equilibration of the triblock copolymers to the desired morphology, membranes with pores were created by removing the PLA beads. For instance, the images in Figs. 2(a)–2(d) depict the methodology for the case of lamella morphology. The pores arising in the above morphologies were then filled with water molecules, as shown in Fig. 1(c). To probe the impact of the chain length of the PEO block on water mobility, we converted some or all of the PLA/PEO beads into water molecules, depending on the chain length of PEO blocks in the systems. For example, all PEO and PLA beads were converted to water beads to render a system in which PEO was absent (referred to as PEO = 0) in the results. To probe the influence of the chain length of PEO blocks on water mobility in the smaller pore size, we converted some of the PLA beads connected to PS into PEO beads.

Since the polymer membranes are intended for use at a temperature below the glass transition of the PS block, in our simulations, the PS blocks were rendered immobile after the water was introduced. Equilibration after water addition was considered to be reached when the density profile of PEO blocks and water particles in the solvated pores exhibited no variations with further simulation time (supplementary material Fig. S1). Simulations in all cases were then run further, for  $10 \times 10^6$  steps in  $0.04 \tau$  time steps, to collect data for analysis.

## C. Analysis

The primary quantity of interest in the present study is the self-diffusion coefficient of water.

### 1. Global diffusion

The isotropically averaged global diffusion coefficient ( $D$ ) was extracted from the slope of the long-time mean squared displacement ( $MSD$ ) of water (supplementary material Fig. S2) using Einstein's relation

$$D = \lim_{t \rightarrow \infty} \frac{1}{6} \frac{d(\langle [r_i(t) - r_i(0)]^2 \rangle)}{dt}, \quad (3)$$

where  $r_i(t)$  is the position of particles at time  $t$ . We also simulated separately the pure bulk water systems and extracted the self-diffusion of bulk water ( $D_B$ ) =  $0.132 r_c^2/t$  (accounting for the simulation box length, as shown in supplementary material Fig. S3). For the diffusivity results that quantify the impact of morphologies along with the PEO chain length, the global diffusion of water ( $D$ ) is normalized by  $D_B$ . In addition, for the systems that vary the chain length of PEO blocks and pore sizes,  $D$  is normalized by the diffusivity values ( $D_0$ ) for the different pore sizes when the PEO chains are absent (PEO = 0). In addition, the solvent-swollen PEO layer heights ( $H_b$ ) were extracted by averaging the end to end distance of PEO chains in the systems relative to the dry PEO layer heights ( $H_{b,dry}$ ).

### 2. Local diffusion

We also computed, as a function of distance from the pore walls, the short-time self-diffusion coefficient of water parallel ( $D_{||}$ ) to the PS interface. Toward this objective, the  $MSDs$  of water molecules were spatially resolved as a function of distance from the PS interface by averaging over the particle's position at each time origin, using a bin width of  $1 r_c$  and 1000 configurations sampled every  $1.0 \tau$ . We computed  $D_{||}$  from the time derivative of the  $MSD$  for  $2\tau \leq t \leq 3\tau$ , which was chosen as the interval during which the particle motion became nearly diffusive but the  $MSD$  was still less than the bin width (supplementary material Fig. S4). The extracted local diffusion coefficient of water was normalized by the diffusion coefficient of water in bulk over this same time window ( $0.124 r_c^2/t$ ). This value was 6% lower than that measured

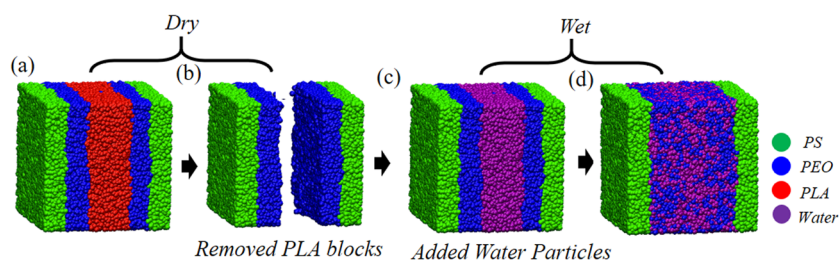


**FIG. 2.** Images of the process for creating and adding water particles in the pore in the (a) lamellae morphology, (b) pore created after removing PLA blocks, (c) initial system (right after adding water particles inside the pore), and (d) final configuration of the system in water. Representative color: green for the PS block, blue for the PEO block, red for the PLA block, and purple for water particles.

from the long-time MSD because the motion was not yet fully diffusive in this window, due in part to the finite time required to propagate hydrodynamic interactions through the periodic boundaries. Nonetheless, when normalized in this way, these short-time measurements provide a reasonable estimate of the local diffusion coefficients.

### III. RESULTS AND DISCUSSION

#### A. Diffusivity of water in different morphologies

We begin our discussion by presenting results that compare the transport properties of water in the pores arising in lamellae, cylinder, and gyroid morphologies (Fig. 3). Comparing the water mobilities in different systems, we observe that the diffusivities follow the order  $D_{\text{Lamellae}} > D_{\text{Gyroid}} > D_{\text{Cylinder}}$ .

To unravel the physics underlying the above results, we first note that in all three morphologies, the transport of the solvent is expected to be constrained to the direction parallel to the interfaces. Hence, transport in lamellar morphologies is expected to closely resemble the diffusion of a penetrant that is constrained to move in only two dimensions. This dimensionality reduction alone is expected to lead to a diffusivity that is two-thirds of the bulk value. Similarly, transport in cylindrical morphologies is expected to resemble diffusion of penetrants confined to move in a single dimension, reducing the diffusivity to one-third of the bulk value. For the case of gyroid morphologies, a combination of dimensionality and tortuosity effects is expected to be in play. A recent study by Shen *et al.*<sup>13</sup> examined the diffusion of a penetrant in gyroid morphologies, and for the construct considered in our study (i.e., the transporting phase corresponding to the inner regions of the gyroid, and for the volume fraction considered), they found that the tortuosity/dimensionality-induced reduction in the diffusivity is on the order of a factor of 0.49. However, we note that the results of Shen *et al.* were based on a periodic gyroid configuration with equilibrium domain spacings; in contrast, our results were based on a single morphology having some nonequilibrium defects.<sup>13</sup>

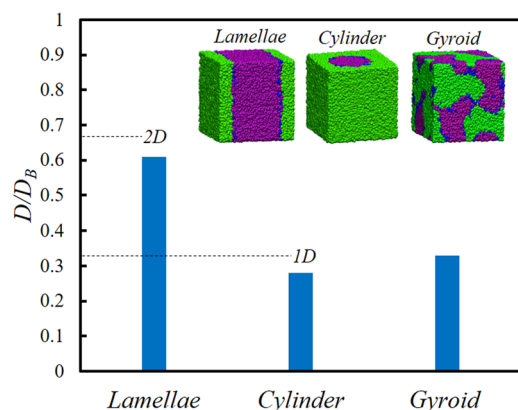


**FIG. 3.** Normalized diffusion coefficient of water in lamellae, cylinders, and gyroids with corresponding images of systems with PEO = 4. Dotted lines in the image show the expected mobility in lamellae and cylinders based on dimensionality considerations.

In comparing the above expectations with our simulation results (the diffusivities, based purely on dimensionality/tortuosity considerations, are indicated by dotted lines in Fig. 3), we observe that a majority of the reductions observed in the diffusivities of water in different morphologies can indeed be explained by the arguments discussed in the previous paragraph. Such results demonstrate that dimensionality/tortuosity considerations constitute the primary origin of the influence of morphology on the transport properties.

However, in Fig. 3, we do observe deviations from the dimensionality-based predictions for lamellae and cylinders. Such results contrast with the outcomes of Shen *et al.*<sup>13</sup> in the context of ion transport in various block copolymer morphologies. Therein, the mobilities probed by the random walk of a point tracer matched with their molecular dynamics results for ion/penetrant diffusion in different morphologies. Such considerations suggest the existence of additional physics that influence the impact of morphology on solvent transport in block copolymer membranes. In Secs. III B and III C, we unravel the mechanisms underlying the deviations noted in Fig. 3 by focusing on the PEO chains and their impact on the dynamics of water molecules. In the remainder of this article, we will use the terminology “ideal” to refer to the diffusivity values expected based solely on dimensionality and tortuosity considerations.

#### B. Influence of PEO chains decorating the pore walls

In an effort to understand the mechanistic origins of deviations from ideality of water diffusivities, we focused on the role of the PEO chains decorating the pore walls. We first considered the lamellar morphology and characterized the averaged diffusivity of water as a function of the PEO chain length in the pores. These results are displayed in Fig. 4, in which deviations from the “ideal” values are seen to increase with an increase in the PEO block length. Such results suggest that the presence of PEO chains plays an important role in influencing deviations from ideal solvent diffusivities and that such deviations increase with an increase in the PEO chain molecular weights.

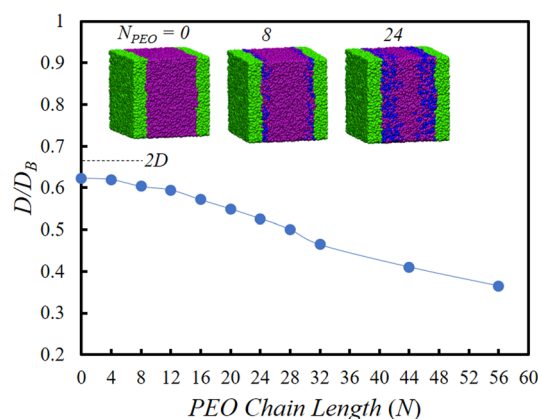


**FIG. 4.** The normalized diffusion coefficient of water as a function of PEO chain lengths in lamellae systems. Inset images show representative lamellae systems for PEO = 0, 8, and 24, as labeled. The dotted line is the expected mobility of particles in an ideal lamella.

To understand the above results, we probed the local densities and the parallel diffusivities of water inside the lamella pores. Figs. 5(a) and 5(b) present the local density profiles of water and PEO inside the pores. By comparing the densities of water and PEO, we see that there is penetration of water into the PEO layer of the pores, which leads to a swelling of the PEO layer. Broadly, three regimes can be noted in the displayed results. At small values of PEO chain lengths (PEO chain lengths  $\leq 8$ ), water nearly penetrates into the PS interface. With an increase in the PEO chain length, the interpenetration between water and PEO is seen to increase, leading to a swelling of the PEO layer relative to the dry PEO brush conditions. The latter result is clearly evident in the normalized swollen brush heights presented in Fig. 5(c), which display a strong dependence on the PEO chain length. However, for PEO chain lengths up to 28, the PEO segments from the opposite layers do not overlap, and hence, the density of water in the middle of the layer is the same as the bulk density of water. For PEO chain lengths  $\geq 28$ , the PEO segments do overlap, leading to a reduction in the density of water in the middle of the layer. Interestingly, for a PEO chain length of 56, we observe that both the PEO segments and the water molecules exhibit an almost constant density profile, indicative of a “blocked” PEO pore filled uniformly with water. In this third regime of PEO chain lengths, we note that the normalized brush heights [Fig. 5(c)] display a less sensitive dependence on the PEO chain length.

In Fig. 5(d), we present the local, parallel diffusivities of water as a function of distance from the PS interfaces. For all PEO chain lengths, the diffusivities of water exhibit strong inhomogeneities as a function of distance from the interface. Explicitly, the diffusivities are the lowest near the lamella interface and increase to bulk/unperturbed values as we move toward the middle region of the lamellae. More pertinently, we observe that the local diffusivities exhibit parallels to the regimes noted in our discussion of water and PEO density profiles.

We hypothesize that the results seen in Fig. 5(d) arise from interactions between water and the water selective PEO blocks present in the pores of the membrane. Indeed, as a consequence of being attached to the PS block, the PEO chains act akin to a grafted polymer layer immersed in a good solvent. In such a scenario, the solvent penetrates the brush and swells the grafted layer [Figs. 5(a)–5(c)]. The solvent beads<sup>32–34</sup> that are present inside the brush experience an additional hydrodynamical frictional force arising from the polymer bead force centers. As a consequence of this hydrodynamical drag, the mobilities of the water molecules inside and in the vicinity of the polymer brush are expected to be lowered.

In qualitative support of the above hypothesis, we note a strong correlation between the inhomogeneities observed in the water diffusivities [Fig. 5(d)] and the density profile of PEO chains, as shown in Fig. 5(b). Moreover, if indeed the reduction in water mobilities arises from friction created by the PEO blocks, we expect that the range of modulation of the local water diffusivities will increase with the length of the PEO blocks. The results displayed in Fig. 5(d) confirm such expectations, thereby lending further support to our hypothesis regarding the mechanism of influence of the PEO chains.

While the above arguments provide a qualitative explanation for the observations in Fig. 5(d), we examine in the Appendix a simple “toy” model for the hydrodynamical effects experienced by the solvent molecules in the PEO lamella pores. The model, continuum by nature, adapts ideas proposed by Milner in a different context and envisions the solvent molecule as a sphere moving through a Brinkman medium of the polymer brush.<sup>35</sup> The mesh size of the latter is abstracted based on the correlation of a polymer solution with a concentration equal to the local PEO monomer concentration. Using the simulation results for the PEO monomer concentration, we obtain the local mobility/diffusivity of the solvent “sphere.” A pore-averaged diffusivity is

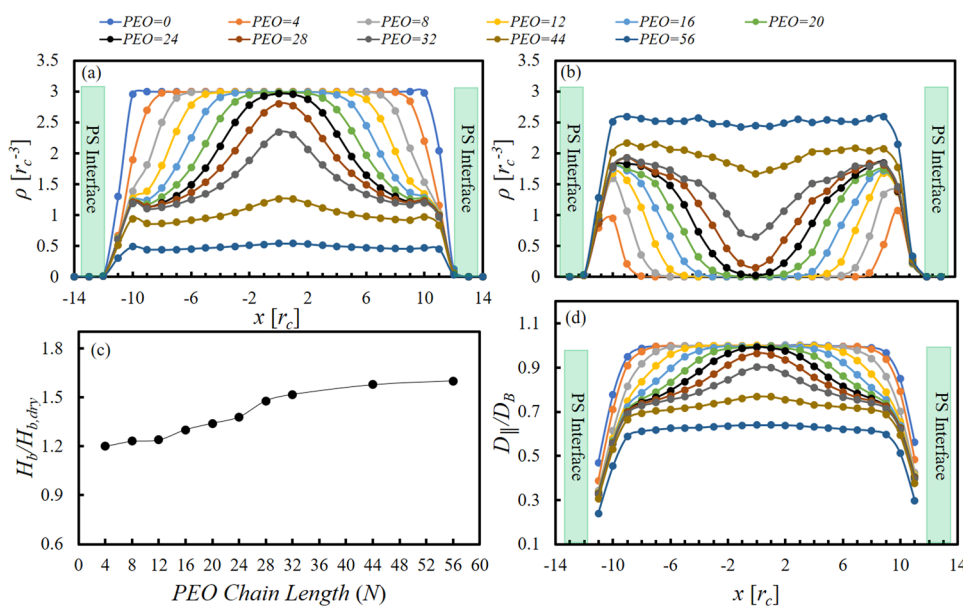


**FIG. 5.** (a) Density profile of water. (b) Density profile of PEO blocks. (c) Swollen PEO brush height normalized by dry brush height. (d) The normalized local diffusion coefficient of water parallel to the lamellae systems in the  $x$ -direction, in the lamellae systems for PEO chain lengths from 0 to 56. The light green shaded region marks the PS interface in the figure.

obtained by averaging the local diffusivity with respect to the solvent density.

The predictions of the above model are compared in Figs. 6(a)–6(c) to simulation results for local diffusivities (results for PEO chain lengths of 44 and 56 are presented in [supplementary material Fig. S5](#)) and in Fig. 6(d) to the averaged diffusivities of the solvent. Despite the simplistic nature of the model, its predictions match quantitatively with computer simulation results, which lend support to our hypothesis regarding the influence of the hydrodynamical friction that arises from the PEO layers.

Since the envisioned experimental framework motivating our study can individually vary the PLA and PEO block sizes (for a fixed volume fraction and size of the PS block), it is possible to exercise independent control over the PEO block size and the width of the lamellae. A relevant issue is whether the PEO-induced deviations of solvent diffusivity from ideality vary independently with the lamella pore size ( $R$ ) and the PEO block size. Since the hydrodynamical influence of PEO chains is expected to scale with the (swollen) brush height  $H_b$ , we expect the (normalized) averaged solvent diffusivities to depend on the ratio  $H_b/R$ . To verify this hypothesis about the role of the pore size, we simulated lamella of different pore sizes containing varying PEO chain lengths and probed the averaged solvent diffusivities as a function of pore sizes and brush heights. Shown in Fig. 7 are our results for these diffusivities (normalized by the respective values for the different pores when PEO chains are absent) depicted as a function of  $H_b/R$ . The results for different pore sizes indeed collapse onto a universal function in this representation, thereby confirming our hypothesis.

Together, the results presented in Figs. 5–7 serve to explain the trends evident in Fig. 4 and demonstrate that the hydrodynamical friction/drag arising from interaction between the solvent and the solvent selective blocks serves as the main source of

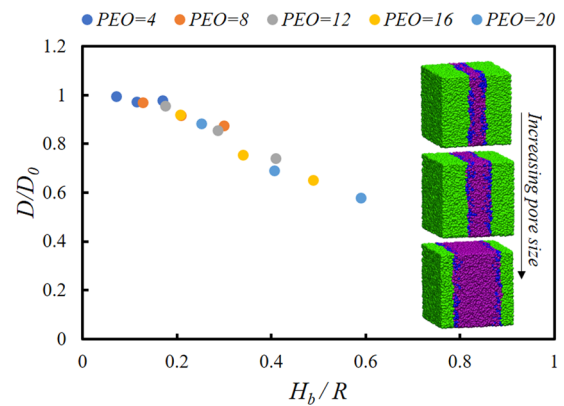


**FIG. 7.** Normalized diffusion coefficient of water as a function of normalized PEO brush height by the pore size in lamellae systems. Inset images show systems with PEO = 8, where the pore size increases from the top to the bottom.

deviation from ideality of solvent diffusivities in block copolymer membranes. Moreover, the results in Fig. 7 demonstrate that the effects of lamella width and PEO chain length can be combined into a single parameter to unravel their influences on solvent diffusivity.

### C. Influence of morphology

To close this discussion of our results, we address the influence of morphology on macroscopic solvent diffusivities. Since the hydrodynamic drag depends on the molecular weight of the PEO chains, decoupling the role of morphology in deviations from ideal values requires that we achieve different morphologies containing

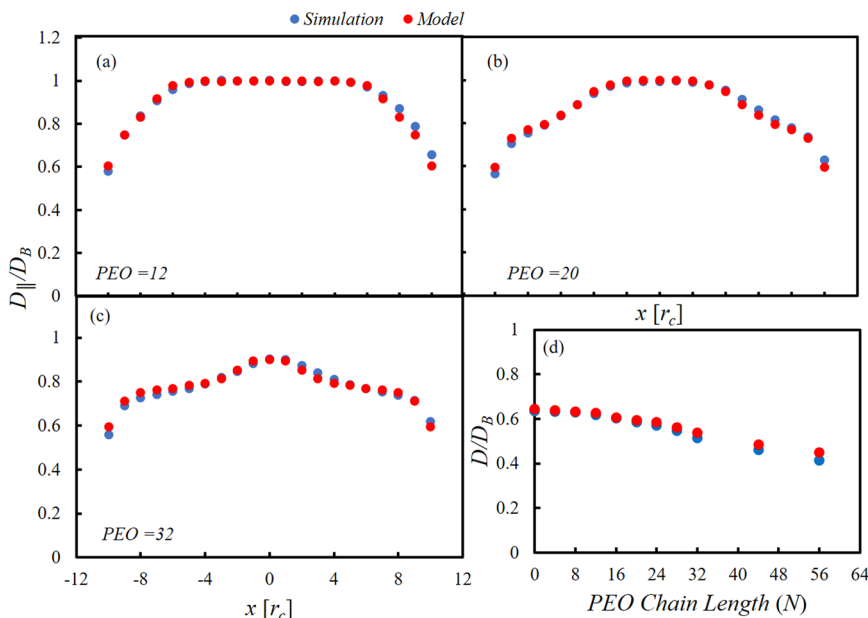


**FIG. 6.** [(a)–(c)] The normalized local diffusion coefficient of water extracted from the “toy” model and DPD simulation [Fig. 5(d)] parallel to the lamellae systems, in the  $x$ -direction in the lamellae systems, for PEO chain lengths of 12, 20, and 32, respectively. (d) The normalized global diffusion coefficient of water from the model and DPD simulation (Fig. 4) as a function of PEO chain length in lamellae systems.

the same number of PEO chains and pore sizes. However, the self-assembly of block copolymers into different morphologies is intimately tied to the volume fraction of the different blocks and, as a consequence, restricts the range of molecular weights of the PEO blocks and pore sizes that can be probed for a specified morphology.

In an effort to address the above issues, we probed the averaged solvent diffusivities in cylindrical morphologies by varying the PEO chain lengths. In Fig. 8(a), we present the normalized solvent diffusivities as a function of PEO chain lengths in cylinder systems. Consistent with the results in Fig. 4 for lamellar systems, the deviation from the “ideal” values increases with an increase in the PEO block length. These results suggest that the deviations from ideality observed for cylindrical morphologies in Fig. 4 originate in hydrodynamical interactions between the PEO chains and the solvent.

We recall that the results in Fig. 7 demonstrated that, for lamellar morphologies, the width of the pore and the PEO (swollen) brush size can be combined into a single parameter to identify their influence on solvent diffusivities. We argued that the physics of solvent PEO interactions are similar in cylindrical morphologies, and we would anticipate similar scaling in quantifying the deviations from ideality observed in cylindrical morphologies. Thus motivated, in Fig. 8(b), we compare the normalized solvent diffusivities for the lamellar and cylindrical morphologies as a function of the ratio of swollen brush height  $H_b$  to the pore diameter  $R$ .

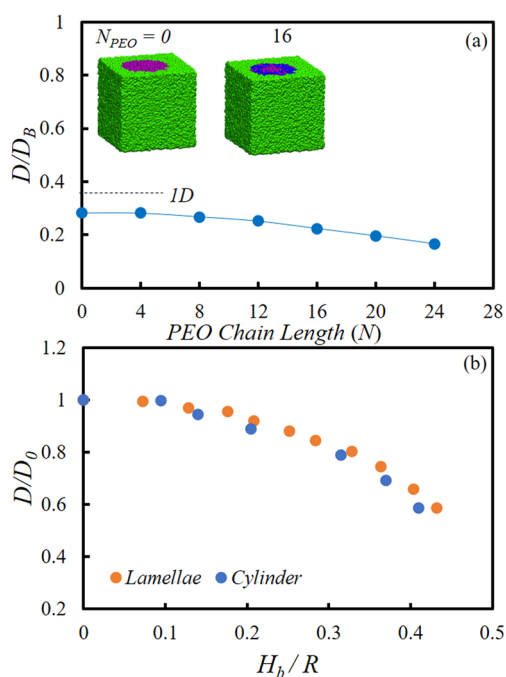


**FIG. 8.** (a) Normalized diffusion coefficient of water as a function of PEO chain length in cylinder systems. Inset images show representative cylinder systems for PEO = 0 and 16, as labeled. The dotted line provides a guideline for expected mobility of particles in the cylinder. (b) Normalized diffusion coefficient of water as a function of normalized PEO brush height by the pore size in cylinder systems.

Surprisingly, it can be seen that the results for the normalized diffusivities of the different morphologies match at a quantitative level in this representation.

Together, the above results suggest that the deviations from ideality noted in Fig. 3 for lamellae and cylinders exhibit a universal dependence on the (swollen) brush height relative to the pore size of the respective morphology. Furthermore, in conjunction with Fig. 3, these results demonstrate that the solvent diffusivities in different block copolymer morphologies are governed primarily by two simple physical aspects, viz., the reduction in diffusivities arising from dimensionality/tortuosity considerations and the hydrodynamical interactions between the solvent and the hydrophilic blocks.

One must however exercise caution in interpreting the outcomes of Fig. 8. Indeed, the morphologies themselves differ in the structural characteristics relating to local solvent densities, the interpenetration between the solvent and PEO layers, and the resulting swollen brush heights. Hence, the extent of deviation from ideality of the averaged solvent diffusivity does exhibit a dependence on the morphologies. However, the results of Fig. 8 demonstrate that, pending knowledge of the structural characteristics specific to the morphology (i.e.,  $H_b$ ), the averaged diffusivities in different morphologies can be rendered onto a universal function.

Do pore size effects similar to those seen for lamellae and cylinders also manifest in gyroid morphologies? To address this issue, we studied the dynamical properties of the gyroid, which has a smaller pore size, and compared them to the results in Fig. 3 (cf. Fig. 9). We refer to “Gyroid-I” for the system shown in Fig. 3 ( $N_{PEO} = 4$ ) and “Gyroid-II” for the new system with a smaller average pore size but the same chain length of PEO blocks ( $N_{PEO} = 4$ ). Consistent with results presented in Fig. 6 for lamellar systems, we observe that narrowing the pore size (for a fixed PEO chain length) reduces the macroscopic water diffusivities in such morphologies.

Can the results for gyroid morphologies be rendered in a representation similar to that of Fig. 8? As evident in Fig. 9, the gyroids in

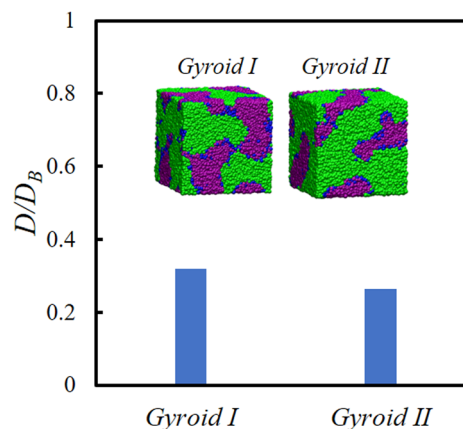


**FIG. 9.** Normalized diffusion coefficient of water for two systems of gyroids. Inset images (top) show corresponding systems. We refer to Gyroid-I and Gyroid-II for systems with different pore shapes and sizes.

our simulations possess nonuniform pore sizes and tortuous channels that arise from nonequilibrium effects (Gyroid I and Gyroid II are themselves morphologically distinct). Even in the context of equilibrated gyroid morphologies, the PEO conformations accompanying such nonuniform pores probably exert an influence on the solvent mobilities that may not be captured by simple hydrodynamical or scaling considerations. Unfortunately, resolving this issue requires characterizing the local dynamics and structure in such nonuniform pores of gyroid morphologies—a complex task that we must defer to future work.

#### IV. CONCLUSIONS

Together, the results presented in this study clearly demonstrate that transport characteristics of solvent in pores that arise from the self-assembled morphologies of block copolymers are modulated by the hydrodynamical influence of the solvent selective blocks in the pore. As a consequence, the dynamical characteristics of solvent inside the pores exhibit strong inhomogeneities relative to the interface. Interestingly, our results demonstrate that, beyond the dimensionality influence arising from confinement in pores, the hydrodynamical effects from the PEO chains can be collapsed into a universal dependence on pore size relative to the brush height. The results presented herein lay the groundwork for building simpler models and coarse-grained approaches for predicting the transport properties of solvents in such nanoporous membranes.

#### SUPPLEMENTARY MATERIAL

See the [supplementary material](#) for  $\chi_{ij}$  and interaction parameters between polymer blocks and water particles (see Tables S1 and S2, respectively), density profile of PEO blocks and water as a function of time, mean squared displacement of water in different directions, diffusion coefficient of bulk water as a function of box length, parallel component of the mean squared displacement of water in each bin size for the local diffusion coefficient, and the local diffusion coefficient of water extracted from the toy model and DPD simulation for PEO chain lengths 44 and 56 (see Figs. S1–S5, respectively).

#### ACKNOWLEDGMENTS

We thank Professor Benny Freeman and other members of M-WET for many useful discussions. We also thank Ms. Pam Cook for suggestions and revisions which improved the stylistic aspects of the preprint. This work was supported by the Center for Materials for Water and Energy Systems, an Energy Frontier Research Center funded by the U.S. Department of Energy, Office of Science, Basic Energy Sciences under Award No. DE-SC0019272. Acknowledgment is also made to the Robert A. Welch Foundation (Grant No. F-1599 to VG and Grant No. F-1696 to TMT). We acknowledge the Texas Advanced Computing Center (TACC) at The University of Texas at Austin for providing HPC resources.

#### APPENDIX: HYDRODYNAMIC MODEL FOR SOLVENT DIFFUSIVITY IN THE PEO

In this section, we provide a short description of the continuum hydrodynamical model underlying the results of Fig. 6. The basis for

such a model is inspired by the work of Milner,<sup>35</sup> who examined the penetration of the shear flow into polymer brushes. In this context, Milner envisioned the polymer brush as a Brinkmann medium with a mesh size equal to that of the correlation length of the polymer solution at the concentration of the brush monomers.

In the present work, we adopted the above picture and envisioned the solvent as a “particle” or radius  $r^*$  diffusing through a Brinkmann medium with a mesh size equal to that of the correlation length of the polymer solution at the concentration of the PEO monomers. We used simulation results for the local concentration of the PEO monomers. Unfortunately, the mesh size ( $\xi$ ) for many of the conditions examined in this study fell either in the range  $\xi \approx r^*$  or  $\xi > r^*$ , regimes that are beyond the limits where a continuum picture of the Brinkmann medium is expected to apply.<sup>36</sup> While new theories and simulations have emerged for such “noncontinuum” regimes,<sup>37–42</sup> we still lack a generally accepted picture. Moreover, considering the simplistic nature of our framework, embedding such complex theories was not consistent with our objective. *In lieu* of such efforts, we used the continuum theory (strictly speaking, valid only for  $r^* \gg \xi$ ) for the diffusivity of a sphere  $D$  in an unbounded Brinkmann medium,

$$\frac{D}{D_0} = \left(1 + \alpha + \frac{1}{9}\alpha^2\right)^{-1},$$

where  $D_0$  denotes the diffusivity of the sphere in a pure solvent and  $\alpha = r^*/\xi$ .

While corrections to the above model have been developed to account for the presence of walls,<sup>43</sup> results have been numerical and beyond the scope of the present work. *In lieu* of such considerations, in order to account for wall effects, we corrected the above local diffusivities by the numerical values of the local solvent diffusivities arising in the case where no PEO chains are present [PEO = 0 in Fig. 5(d)]. Using the above model, a nominal value of  $r^* = r_c/2$ , and the local volume fractions of PEO, we estimated the local diffusivities depicted in Figs. 6(a)–6(c).

#### REFERENCES

- <sup>1</sup>F. S. Bates and G. H. Fredrickson, *Phys. Today* **52**(2), 32 (1999).
- <sup>2</sup>F. Bates, *Annu. Rev. Phys. Chem.* **41**, 525 (1990).
- <sup>3</sup>J. M. Milhaupt and T. P. Lodge, *J. Polym. Sci., Part B: Polym. Phys.* **39**, 843 (2001).
- <sup>4</sup>M. W. Hamersky, M. A. Hillmyer, M. Tirrell, F. S. Bates, T. P. Lodge, and E. D. von Meerwall, *Macromolecules* **31**, 5363 (1998).
- <sup>5</sup>O. Oparaji, M. Minelli, C. Zhu, E. Schaible, A. Hexemer, and D. T. Hallinan, *Polymer* **120**, 209 (2017).
- <sup>6</sup>P. J. Griffin, G. B. Salmon, J. Ford, and K. I. Winey, *J. Polym. Sci., Part B: Polym. Phys.* **54**, 254 (2016).
- <sup>7</sup>J. H. Choi, C. L. Willis, and K. I. Winey, *J. Membr. Sci.* **394–395**, 169 (2012).
- <sup>8</sup>J. L. Thelen, S. Inceoglu, N. R. Venkatesan, N. G. Mackay, and N. P. Balsara, *Macromolecules* **49**, 9139 (2016).
- <sup>9</sup>A. A. Rojas, S. Inceoglu, N. G. Mackay, J. L. Thelen, D. Devaux, G. M. Stone, and N. P. Balsara, *Macromolecules* **48**, 6589 (2015).
- <sup>10</sup>N. P. Balsara and J. Newman, *J. Chem. Educ.* **90**, 446 (2013).
- <sup>11</sup>V. Sethuraman, S. Mogurampelly, and V. Ganesan, *Macromolecules* **50**, 4542 (2017).
- <sup>12</sup>V. Sethuraman, S. Mogurampelly, and V. Ganesan, *Soft Matter* **13**, 7793 (2017).
- <sup>13</sup>K. H. Shen, J. R. Brown, and L. M. Hall, *ACS Macro Lett.* **7**, 1092 (2018).

- <sup>14</sup>M. S. Alshammasi and F. A. Escobedo, *Soft Matter* **15**, 851 (2019).
- <sup>15</sup>L. Y. Schneider and M. Müller, *Macromolecules* **52**, 2050 (2019).
- <sup>16</sup>A. S. Zalusky, R. Olayo-Valles, C. J. Taylor, and M. A. Hillmyer, *J. Am. Chem. Soc.* **123**, 1519 (2001).
- <sup>17</sup>D. T. Cooney, M. A. Hillmyer, E. L. Cussler, and G. D. Moggridge, *Crystallogr. Rev.* **12**, 13 (2006).
- <sup>18</sup>R. D. Groot and P. B. Warren, *J. Chem. Phys.* **107**, 4423 (1997).
- <sup>19</sup>R. D. Groot and T. J. Madden, *J. Chem. Phys.* **108**, 8713 (1998).
- <sup>20</sup>M. T. Lee, A. Vishnyakov, and A. V. Neimark, *J. Chem. Theory Comput.* **11**, 4395 (2015).
- <sup>21</sup>M. T. Lee, A. Vishnyakov, and A. V. Neimark, *J. Phys. Chem. B* **117**, 10304 (2013).
- <sup>22</sup>D. Aryal and V. Ganesan, *J. Chem. Phys.* **149**, 224902 (2018).
- <sup>23</sup>S. Plimpton, *J. Comput. Phys.* **117**, 1 (1995).
- <sup>24</sup>P. J. Hoogerbrugge and J. M. V. A. Koelman, *Europhys. Lett.* **19**, 155 (1992).
- <sup>25</sup>P. Sandhu, J. Zong, D. Yang, and Q. Wang, *J. Chem. Phys.* **138**, 194904 (2013).
- <sup>26</sup>B. Abu-Sharkh and A. Alsunaidi, *Macromol. Theory Simul.* **15**, 507 (2006).
- <sup>27</sup>A. Maiti and S. McGrother, *J. Chem. Phys.* **120**, 1594 (2004).
- <sup>28</sup>H. Mao and M. A. Hillmyer, *Macromol. Chem. Phys.* **209**, 1647 (2008).
- <sup>29</sup>A. Takhulee, Y. Takahashi, and V. Vao-soongnern, *J. Polym. Res.* **24**, 8 (2016).
- <sup>30</sup>M. T. Lee, R. Mao, A. Vishnyakov, and A. V. Neimark, *J. Phys. Chem. B* **120**, 4980 (2016).
- <sup>31</sup>C. A. Tyler, J. Qin, F. S. Bates, and D. C. Morse, *Macromolecules* **40**, 4654 (2007).
- <sup>32</sup>S. Minko, I. Luzinov, V. Luchnikov, M. Müller, S. Patil, and M. Stamm, *Macromolecules* **36**, 7268 (2003).
- <sup>33</sup>C. Pastorino, K. Binder, and M. Müller, *Macromolecules* **42**, 401 (2009).
- <sup>34</sup>D. I. Dimitrov, A. Milchev, and K. Binder, *J. Chem. Phys.* **127**, 084905 (2007).
- <sup>35</sup>S. T. Milner, *Macromolecules* **24**, 3704 (1991).
- <sup>36</sup>L. H. Cai, S. Panyukov, and M. Rubinstein, *Macromolecules* **44**, 7853 (2011).
- <sup>37</sup>S. A. Egorov, *J. Chem. Phys.* **134**, 084903 (2011).
- <sup>38</sup>R. Chen, R. Poling-Skutvik, M. P. Howard, A. Nikoubashman, S. A. Egorov, J. C. Conrad, and J. C. Palmer, *Soft Matter* **15**, 1260 (2019).
- <sup>39</sup>R. Chen, R. Poling-Skutvik, A. Nikoubashman, M. P. Howard, J. C. Conrad, and J. C. Palmer, *Macromolecules* **51**, 1865 (2018).
- <sup>40</sup>V. Pryamitsyn and V. Ganesan, *J. Polym. Sci., Part B: Polym. Phys.* **54**, 2145 (2016).
- <sup>41</sup>V. Pryamitsyn and V. Ganesan, *Phys. Rev. Lett.* **100**, 128302 (2008).
- <sup>42</sup>V. Ganesan, V. Pryamitsyn, M. Surve, and B. Narayanan, *J. Chem. Phys.* **12**, 221102 (2006).
- <sup>43</sup>J. Feng, P. Ganatos, and S. Weinbaum, *J. Fluid Mech.* **375**, 265 (1998).